© American Society for Mass Spectrometry, 2016

CrossMark

J. Am. Soc. Mass Spectrom. (2016) 27:908–916
DOI: 10.1007/s13361-016-1353-9

RESEARCH ARTICLE

Hybrid Organic/Inorganic Materials Depth Profiling Using Low Energy Cesium Ions

Céline Noël, Laurent Houssiau

Research Centre in Physics of Matter and Radiation, University of Namur, Namur, Belgium

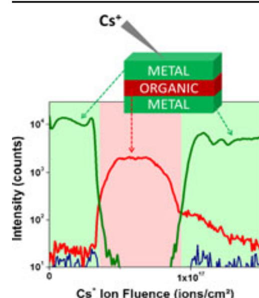

Abstract. The structures developed in organic electronics, such as organic light emitting diodes (OLEDs) or organic photovoltaics (OPVs) devices always involve hybrid interfaces, joining metal or oxide layers with organic layers. No satisfactory method to probe these hybrid interfaces physical chemistry currently exists. One promising way to analyze such interfaces is to use in situ ion beam etching, but this requires ion beams able to depth profile both inorganic and organic layers. Mono- or diatomic ion beams commonly used to depth profile inorganic materials usually perform badly on organics, while cluster ion beams perform excellently on organics but yield poor results when organics and inorganics are mixed. Conversely, low energy Cs^+ beams (<500 eV) allow organic and inorganic materials depth profiling with comparable erosion rates. This paper shows a successful depth profiling of a model hybrid system made of metallic (Au, Cr) and organic (tyrosine) layers, sputtered with 500 eV Cs^+ ions. Tyrosine layers capped with metallic overlayers are depth profiled easily, with high intensities for the characteristic molecular ions and other specific fragments. Metallic Au or Cr atoms are recoiled into the organic layer where they cause some damage near the hybrid interface as well as changes in the erosion rate. However, these recoil implanted metallic atoms do not appear to severely degrade the depth profile overall quality. This first successful hybrid depth profiling report opens new possibilities for the study of OLEDs, organic solar cells, or other hybrid devices.
Keywords: Organic electronics, OLEDs, OPVs, Hybrid materials, SIMS, Cesium, Depth profiling

Received: 15 October 2015/Revised: 21 January 2016/Accepted: 23 January 2016/Published Online: 16 February 2016

Introduction

Time-of-Flight Secondary Ion Mass Spectrometry (ToF-SIMS) has been repeatedly used to depth profile inorganic and, more recently, organic samples. An increasing amount of literature demonstrates that polyatomic primary ions such as SF_5^+, C_{60}^+, and Ar_n^+ are suitable for this purpose [1–6]. The total energy is shared by each atom in the cluster, limiting the penetration depth and thereby the extent of the chemically damaged layer under the surface. Owing to their high sputtering yield, these ions show a high cleaning efficiency and thus avoid damage accumulation on materials removed layer-by-layer [7–9].

Recently, hybrid samples (organic *and* inorganic multilayers) have played an important role in a broad range of fields, especially in microelectronics with the development of OLEDs and organic solar cells. Other application fields include catalyst devices for air or water purification [10] and assemblies containing hybrid metal/polymer interfaces used in the automotive and aviation industry. Presently, the challenge is to further improve their performances (lifetime, stability, etc.) by understanding the phenomena that occur at the interfaces inside their multilayer structure (interlayer diffusion or degradation mechanisms depending on illumination, temperature variations, and atmospheric conditions [11, 12]). Despite their excellent performance on organic samples, cluster ions are rather inefficient to depth profile inorganic samples [13], so that it remains a challenge to use them efficiently on hybrid samples [14]. The main issue for this type of analysis is the extreme sputter rate difference between organics and inorganics [15]. The literature reports three different ways to obtain depth profiles on hybrid systems. The first approach consists on removing the inorganic layers from the device, and to subsequently analyze the remaining organic parts with cluster ion beams. This has been performed for instance on OLED systems, in which the metallic cathode is removed mechanically before the organic layers analysis [16]. Another approach consists on switching ion sources while crossing hybrid interfaces (e.g., using a monoatomic Ar source on inorganic layers, then switching to Argon cluster ion beams in the organic layers [17]). Finally, hybrid depth profiling with only one source has been attempted on 1.4 to 3.5 nm gold layer embedded in cholesterol deposits

Correspondence to: Laurent Houssiau; *e-mail:* Laurent.houssiau@unamur.be

[14], sputtered with C_{60}^+ ion source. On these model systems, the organic layer shows an important molecular ion signal decrease after the gold is removed. Regardless of the metal layer thickness, fragmentation enhancement is observed, as well as a decrease of both the sputtering yield and cleanup efficiency, compared with the upper cholesterol layer.

In this context, we managed to assess the impact of low energy Cs^+ as a sputter source for hybrid organic/inorganic samples depth profiling. Cs high reactivity ensures a negative ion signal enhancement, along with free radicals scavenging [18]. This source already proved its efficiency on both inorganics [19–22] and organics [23–25]. In this paper, we analyze model systems made of different metals (gold or chromium) and tyrosine multilayer systems deposited on silicon substrates. We show how it is possible not only to reach the silicon substrate with a single set of parameters, but also to keep a high intensity for the deprotonated tyrosine molecular ion even after sputtering through 10 nm gold or chromium.

Experimental

Sample Description

Hybrid multilayer samples consist of gold or chromium layers grown by physical vapor deposition (PVD) and evaporated tyrosine (denoted "Tyr" below) on silicon substrates.

Silicon substrates <100> were purchased from Si-Mat (Kaufering, Germany). Prior to analysis, they were cut into 1 cm dices and cleaned by sonicating them in an isopropanol bath for 15 min. Then they were immediately dried under a nitrogen flow.

L-tyrosine ($C_9H_{11}NO_3 \geq 97$ %) purchased from Sigma-Aldrich Belgium (Diegem, Belgium) was deposited by thermal evaporation in a Cressington Evaporation Supply LT 1500 308R (Watford, UK). The chamber was first brought to a 10^{-7} mbar pressure. The crucible containing the tyrosine powder was then heated up to 330–350 °C. The pressure during evaporation never exceeded 10^{-6} mbar and the deposited thickness was controlled by a quartz microbalance, which was calibrated with ellipsometry and profilometry in turn.

Gold and chromium layers were grown by PVD with a Quorum Q150 T E/S device from Quorum Technologies (Laughton, UK), from which sputter targets were also purchased. Twenty and 120 mA currents were used for Au and Cr, respectively. The distance between the target and the sample was 50 mm. The layer thickness was once again measured with a Quartz microbalance and calibrated with a profilometer.

Using these disposition approaches, the following metal/organic systems were prepared:

- One-layer samples for sputtering yields measurements (Tyr/Si), (Cr/Si), and (Au/Si)
- Two-layer samples (10 nm Cr/94 nm Tyr/Si), (92 nm Tyr/10 nm Cr/Si), (10 nm Au/92 nm Tyr/Si), and (92 nm Tyr/10 nm Au /Si)
- Three-layer samples (92 nm Tyr/10 nm Au/92 nm Tyr/Si), (92 nm Tyr/10 nm Cr/94 nm Tyr/Si)

ToF-SIMS Measurements

ToF-SIMS depth profiles were acquired in dual beam mode [26] using a ToF-SIMS IV (Ion-Tof GmbH, Münster, Germany). The analysis beam (Bi_3^+ at 25 keV; current: ~25 pA, pulse width: 20 ns; pulse width after bunching: 0.75 ns; repetition rate: 10 kHz), rastered over a 300 × 300 µm² area and the erosion beam (Cs^+ at 500 eV, current: 37–41 nA), rastered over a 500 × 500 µm² area were operated in noninterlaced mode with one analysis frame (1.6384 s), 10 s erosion, and 1 s pause per cycle, both with a 45° incidence angle to the sample surface. A low energy flood gun ensured charge compensation. The secondary ions were extracted at a 2 kV acceleration voltage. The spectra were calibrated with C_5^-, $C_8H_7O^-$ and $C_9H_{10}NO_3^-$ peaks and were acquired from 0 to 880 *m/z*. The mass resolution (m/Δm) at the $C_9H_{10}NO_3^-$ (*m/z* 180) and Si^- (m/z 28) peaks were typically above 8500 and 10,500 in negative ion polarity. Ion intensities in depth profiles are expressed in ions/cycle units (simply denoted by "counts" in the graphs), which is the number of ions of a given species detected per analysis cycle, lasting 128 × 128 × 10^{-4} s, or 1.6384 s.

Sputtering Yields

The sputtering yields of single layers deposited on Si were determined by using the following relation (Equation 1):

$$Y = \frac{eAd}{It} \quad (1)$$

where e stands for the electron charge (1.6 × 10^{-19} C/ion), A is the sputtered area in nm², d is the layer thickness in nm, determined by profilometry, I indicates the sputtering current and t is the time necessary to reach 50% of the steady state intensity of the following layer characteristic signal.

Results and Discussion

Organics on Metals

The depth profile results for the Tyr/Au/Si system are shown in Figure 1a and the results for the Tyr/Cr/Si system are shown in Figure 1b. As expected, both the tyrosine [27] and inorganic films are easily depth profiled with 500 eV Cs^+, with a very sharp interface. The Tyr layer is readily identified with a $C_9H_{10}NO_3^-$ molecular ion or $[Tyr\text{-}H]^-$, at *m/z* 180. Other characteristic fragments are also monitored: $C_8H_8NO^-$ at *m/z* 134, $C_8H_7O^-$ at *m/z* 119 (not shown) and $C_6H_5O^-$ at *m/z* 93 (not show). The molecular ion $[Tyr\text{-}H]^-$ signal drops rapidly at the beginning of the depth profiles, then it rises to reach a steady state value. Intensity oscillations are also noticed at the organic/metal interface. This behavior is common with low energy Cs^+

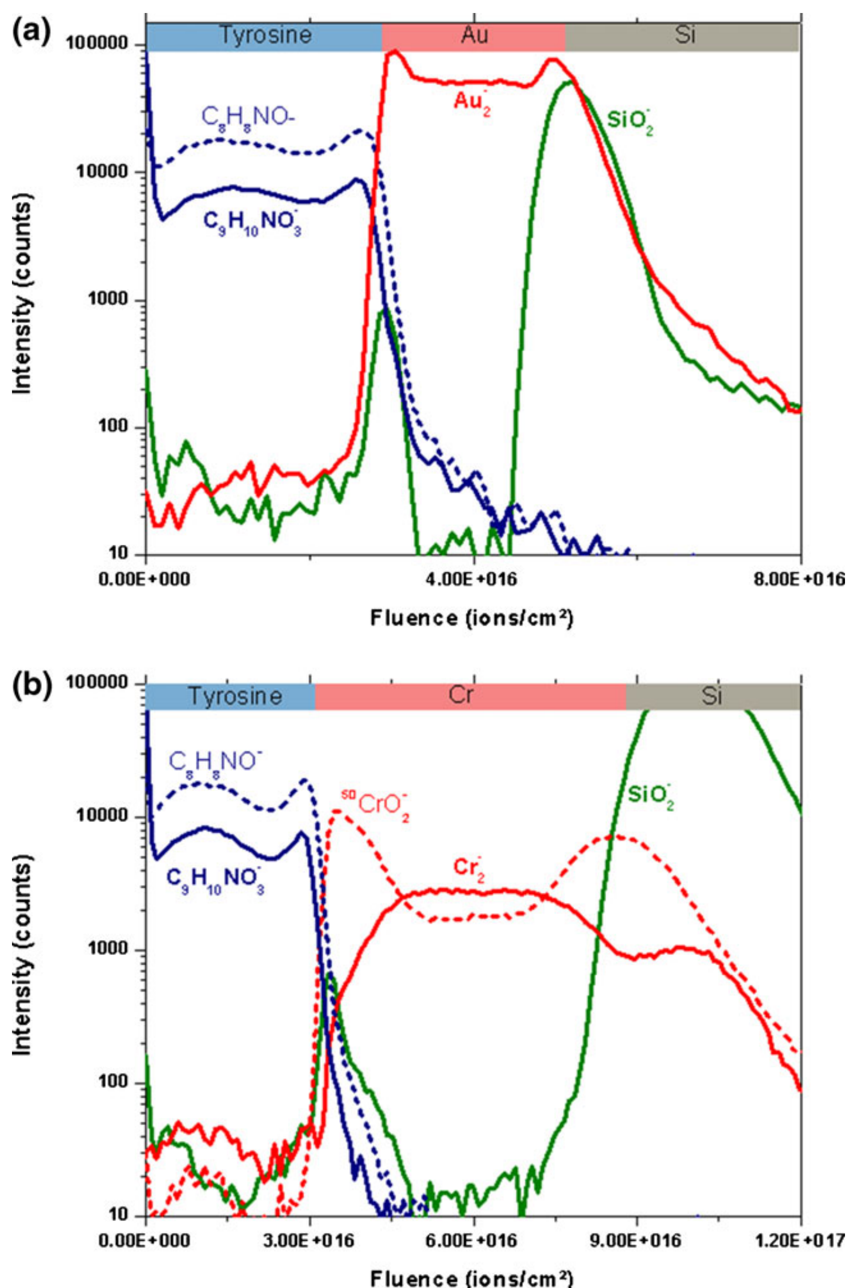

Figure 1. 500 eV Cs^+ depth profiling of 92 nm Tyr/ 10 nm Au/Si multilayers **(a)** and 92 nm Tyr/10 nm Cr/Si multilayers **(b)**

depth profiling as was shown in previous works [18, 24]. The initial drop is caused by rapid fragmentation of the Tyr molecules induced by the Cs^+ ions, leading to the formation of free radicals. When the sputtered depth reaches that of the implanted Cs atoms, reactions between Cs atoms and the free radicals quench the chemical damage processes, such as crosslinking or hydrogen abstraction. Closer to the hybrid interface, Cs concentration variations occur, leading to transients in the molecular signal, possibly related to changes in the negative ionization probability.

The Au signal plotted in Figure 1a is represented by the gold dimer Au_2^-, as opposed to the monomer Au^-, because the Au^- ions saturate the detector. The Cr signal in Figure 1b is also represented by the dimerized Cr_2^- signal. The ion $^{50}CrO_2^-$ at *m/z* 82, plotted in Figure 1b, is a marker for native chromium oxide layers. In both cases, no metal (Cr, Au) is detected in the Tyr layer, meaning that no significant diffusion of metal occurs into the organic layer. The second interface (metal/Si) is identified with a SiO_2^- ion (native oxide).

Metal on Organics

Metal on organic films are much more challenging hybrid systems to characterize with ToF-SIMS compared with the

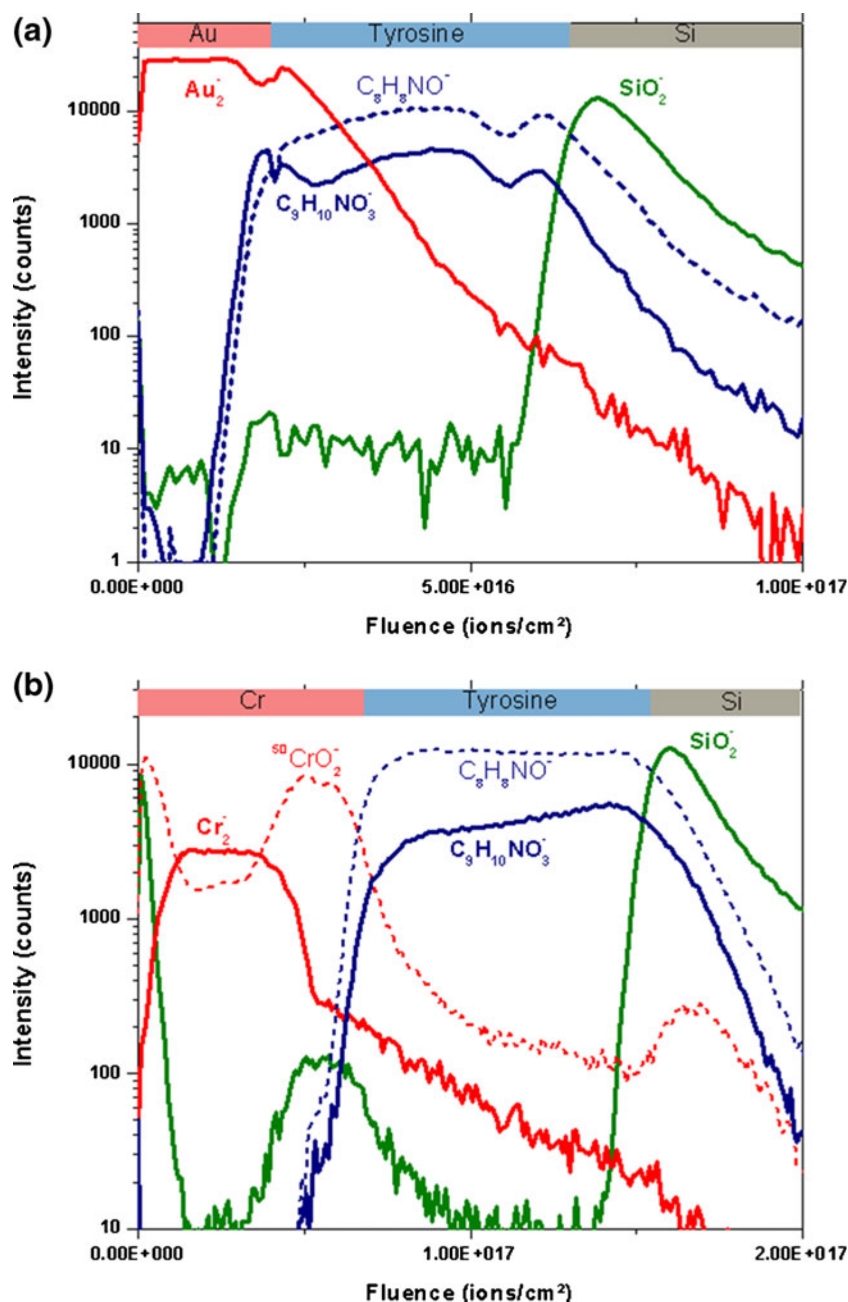

Figure 2. 500 eV Cs^+ depth profiling of 10 nm Au/ 92 nm Tyr/Si multilayers **(a)** and 10 nm Cr/94 nm Tyr/Si multilayers **(b)**

converse situation (organic on metal films). This is because the energetic metal atoms in the collision cascade are injected into the softer and less dense underlying Tyr layer, where they produce extensive molecular damage. Figure 2a shows the depth profile obtained with 500 eV Cs^+ on the Au/Tyr/Si system. The first remarkable observation is the sharp rise of the [Tyr-H]$^-$ signal at the Au/Tyr interface, followed by a high and slightly fluctuating intensity of the molecular ion within the Tyr layer. The Au_2^- intensity remains constant within the Au overlayer, then drops exponentially in the Tyr layer, indicating a broad ion beam induced diffusion of metal into the organic layer. This diffusion is not observed in the reverse layer (Tyr/Au) and is therefore attributable to collisions between the incident Cs^+ ions and Au atoms, pushing these atoms deeper into the Tyr underlayer. This experiment demonstrates that Tyr molecules withstand the collisions with Au atoms with relatively low damage. The initial Tyr intensity drop beyond the Au/Tyr interface could be due to Tyr molecules fragmentation. However, the signal tends to increase deeper in the Tyr layer, where the Au concentration is lower, which strongly limits the collisions between Au atoms and Tyr molecules. The intensity drop measured at the Au/Tyr interface for all secondary ions is

attributed to a temporary charging effect arising when crossing the interface from the highly conductive gold layer to the insulating Tyr layer. This leads to a brief loss of total secondary ion emission and also to sudden peak shifts, which are taken into account in the plotted peak areas.

Figure 2b shows the depth profile obtained with 500 eV Cs^+ in the Cr/Tyr/Si system. Once again, the Tyr signal, monitored by the $[Tyr\text{-}H]^-$ ion, as well as the $C_8H_8NO^-$ fragment, rises rapidly at the Cr/Tyr interface, up to a steady-state, proving that the molecular depth profiling remains efficient beyond the metallic overlayer. The Cr layer is identified by means of Cr_2^- ions at *m/z* 52 and $^{50}CrO_2^-$ ions at *m/z* 82. The Cr_2^- profile is flat in the Cr layer. Then it decreases slowly in the Tyr layer, suggesting again an intensive ion beam induced diffusion of Cr atoms into the Tyr layer. Like in the previous case (Au/Tyr), this diffusion is produced by recoiling the Cr atoms with incident Cs^+ ions deeper through the organic layer. The chromium layer oxidation is measured by means of $^{50}CrO_2^-$ ions. Chromium appears to be oxidized at its surface (native oxide layer) and at the Cr/Tyr interface.

Organic/Metal/Organic/Si Multilayers

Trilayer systems offer two hybrid interfaces (organic/inorganic and inorganic/organic), thereby allowing a direct comparison of molecular signals before crossing the metal film (top Tyr layer) and after crossing the metal film (buried Tyr layer). The depth profile obtained with 500 eV Cs^+ on the Tyr/Au/Tyr/Si system is shown in Figure 3a. Once again, the hybrid depth profiling is successful when looking at the $[Tyr\text{-}H]^-$ peak and all the Tyr related fragments (only the $C_8H_8NO^-$ fragment at *m/z* 134 is shown in Figure 3a). The $[Tyr\text{-}H]^-$ steady-state intensity reaches about 6000 ions/cycle in the first layer, then drops sharply, as expected, at the Tyr/Au interface. Furthermore, the signal rises again sharply at the Au/Tyr interface and then reaches a maximum intensity ca. 4000 ions/cycle. Naturally, the signal decreases again when reaching the Si substrate. Similar conclusions can be drawn for the large fragment at *m/z* 134, with a maximum intensity still exceeding 10,000 ions/cycles in the second Tyr layer. The Au_2^- signal also helps to identify the Au layer and to estimate the Au ion beam induced diffusion through the Tyr layer. The signal rise at the first interface is extremely sharp, but its decay is slow beyond the second interface, as noticed in Figure 2a. The high amount of Au atoms injected in the Tyr layer evidently increases molecular damage, but the molecular signal loss beyond the 10 nm thick Au layer remains quite limited. Compared with the bilayer shown in Figure 2a, a residual Tyr signal is still detected within the Au layer. The reason might be that Au layers evaporated on a Tyr substrate exhibit some defects, such as pinholes, compared with Au layers evaporated on Si.

The depth profile obtained with 500 eV Cs^+ in a Tyr/Cr/Tyr/Si system is shown in Figure 3b. The general features are similar to the previous profile (Figure 3a), with a high $[Tyr\text{-}H]^-$ ion intensity in the first layer (~6000 counts/cycle), a sharp drop at the first interface, followed by another sharp rise at the second interface and an immediate molecular signal recovery. Some oscillations are observed, until the signal reaches a maximum around 1300 counts/cycle, which is lower than in the Tyr/Au/Tyr case, but still remains adequate for molecular depth profiling. Again, an extensive Cr ion beam induced diffusion (followed by Cr_2^- and $^{50}CrO_2^-$ ions) is observed. In order to understand the origin of the Tyr signal intensity oscillations, 3D imaging data (not shown) was reconstructed in the second interface region. It turns out that the intensity loss is related to dark spots observed on all secondary ion images (i.e., areas where the secondary ion intensity is depressed). This is most likely due to differential charging effects at the metal/insulator interface, which are temporarily not fully compensated by electron flooding.

Discussion

Metal Injection in the Organic Layer

The key issue in metal/organics depth profiling is the injection of metal atoms into organic layers [28]. In the systems analyzed here, Cr and Au atoms are recoiled from the metallic overlayer through the Tyr layer. As shown in Figures 2 and 3, the Cr and Au ion beam-induced diffusion is evident on the depth profiles, with a long exponential tail observed for all Cr- and Au-containing ions. Figure 4 compares the intensity decay of Au^- and Cr^- ions into the Tyr layer for bilayers (Au or Cr/Tyr). The horizontal scale is now a depth scale calibrated such as the Tyr layer thickness is 92 nm for Au and 94 nm for Cr. The Au^- ions saturate the detector at high concentration (dashed line in Figure 4). Then the signal follows an exponential decay deeper in the Tyr layer. Assuming that the Au or Cr decay obeys the law (Equation 1):

$$I(x) = I_0 \exp\left(-x / d_{\mathrm{Au\ or\ Cr}}\right), \tag{2}$$

where $I(x)$ is the secondary ion intensity, I_0 is a constant, x is the depth and $d_{Au\ or\ Cr}$ is the decay length, which can be measured from depth profiles. From the experiments shown in Figure 4, the decay length for Au atoms is $d_{Au} = 12$ nm, whereas for Cr it is $d_{Cr} = 33$ nm. Therefore, Cr atoms appear to be knocked in much more extensively than Au atoms upon the Cs^+ impact. The energetic metal atoms penetrating the Tyr layer are atoms in motion in the deepest part of the collision cascade initiated in the metal layer upon the Cs^+ impact. We therefore performed SRIM [29] simulations to roughly estimate if a metal is more injected than the other. Two layers are considered in the model: a thin metal (Cr or Au) layer on top of a stoichiometric $C_9H_{11}NO_3$ layer. Figure 5 shows the recoil distribution of Cr and Au for a 1 nm metal overlayer, expressed as an atomic concentration per fluence unit: (atoms/cm³)/(Cs^+ ions/cm²). It appears that significantly more Cr atoms are recoiled just below the interface than Au atoms. It is also

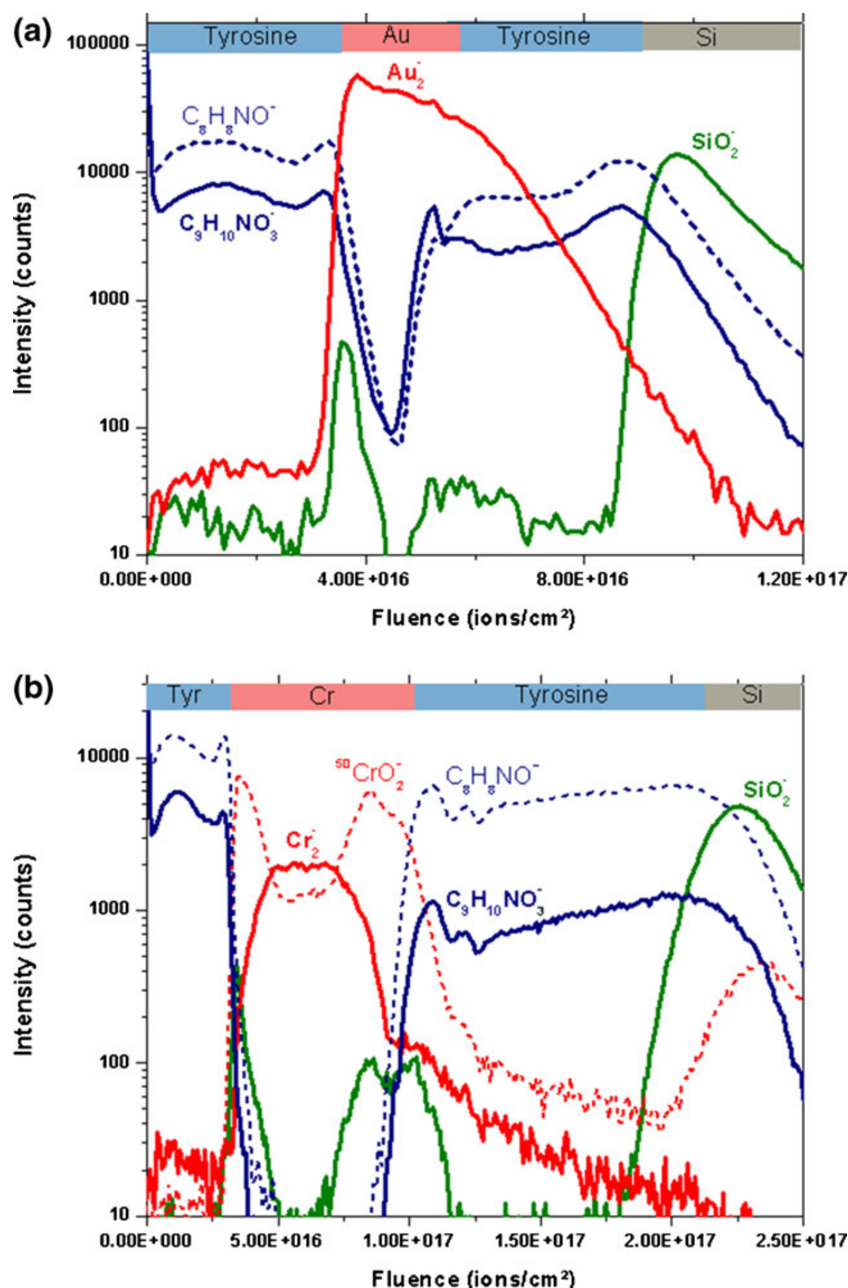

Figure 3. 500 eV Cs^+ depth profiling of 92 nm Tyr/10 nm Au/92 nm Tyr/Si multilayers **(a)** and 92 nm Tyr/10 nm Cr/94 nm Tyr/Si multilayers **(b)**

the case for 0.5 and 1.5 nm simulated metallic layers (not shown). For metallic layers thicker than 2 nm, no Cr or Au atoms are recoiled beyond the interface, since the layer thickness exceeds that of the collision cascade. Moreover, the fluence needed to sputter a given depth of Cr is about three times larger than for an Au layer, so that the atomic Cr concentration below the hybrid interface must be about one order of magnitude higher than the Au concentration. Differences in the depth profiles between Cr and Au are therefore interpreted by assuming that the Tyr layer is much more affected by beam injected Cr atoms than by Au atoms.

Sputtering Yields

Table 1 shows the differences in sputtering yields observed between Tyr and metals, depending on whether they are part of the one-layer, two-layer, or the three-layer samples.

The sputtering yield of pure metals under a 500 eV Cs^+ bombardment is 5.0×10^{-2} nm³/ion (or 3.0 atoms/ion) for gold and 1.6×10^{-2} nm³/ion (or 1.3 atom/ion) for chromium. This matches the values estimated with the SRIM code, which are 3.1 atoms/ion for gold and 1.4 atom/ion for chromium. The sputtering yield measured on Tyr layers is 2.8×10^{-1} nm³/ion: it is only 5.5 times higher than for Au, and 17 times higher than

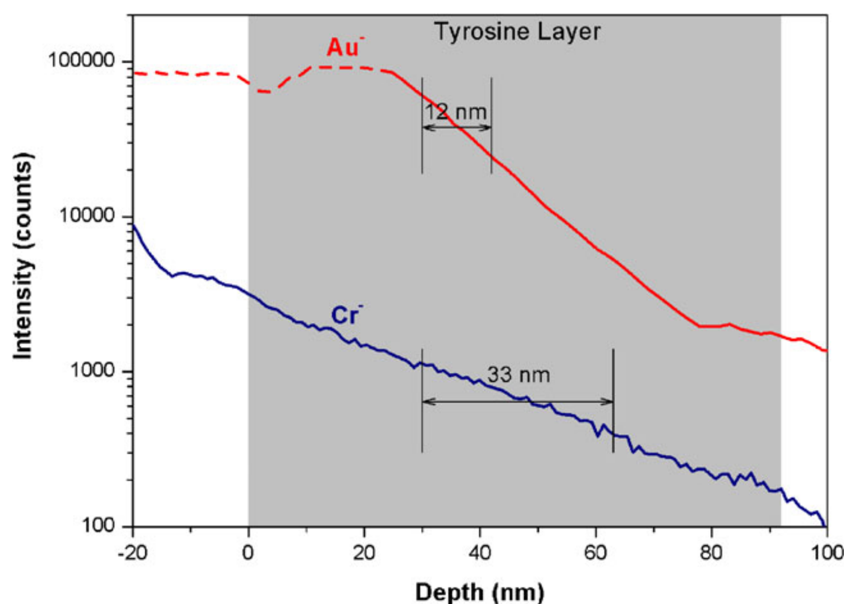

Figure 4. Measurement of the decay length of metallic ions in the tyrosine layer, for bilayers Au or Cr/Tyr sputtered with 500 eV Cs^+ ions

for Cr. The sputtering yield gap between organics and inorganics when using low energy Cs^+ is therefore relatively low compared with the gap observed when using cluster ion beams, which can be as high as two [14] to three [15] orders of magnitude.

The Tyr layer sputtering yield after crossing a metallic layer was also measured. In the Tyr/Au/Tyr structure, the buried Tyr layer surprisingly keeps the same sputtering yield as the top Tyr layer. On the other hand, when Au is replaced by Cr, the sputtering yield of the second Tyr layer is reduced by a factor of three, down to 8.2×10^{-2} nm³/ion. The reasons for this sputtering yield decrease might be related to the high Cr injection in the organic layer combined with the high sputtering yield gap between Cr and Tyr. The sputtering yield does not vary abruptly from a low level in the metal to a high level in the Tyr, but it should rather increase gradually, since the Cr concentration below the interface remains high. The sputtering is slowed down by the high concentration of low sputtering yield Cr atoms, at least close to the metal/organic interface. It probably increases deeper into the layer, where the Cr concentration becomes lower. The sputtering yield reported here is an average over the second (94 nm) Tyr layer: although it is three times

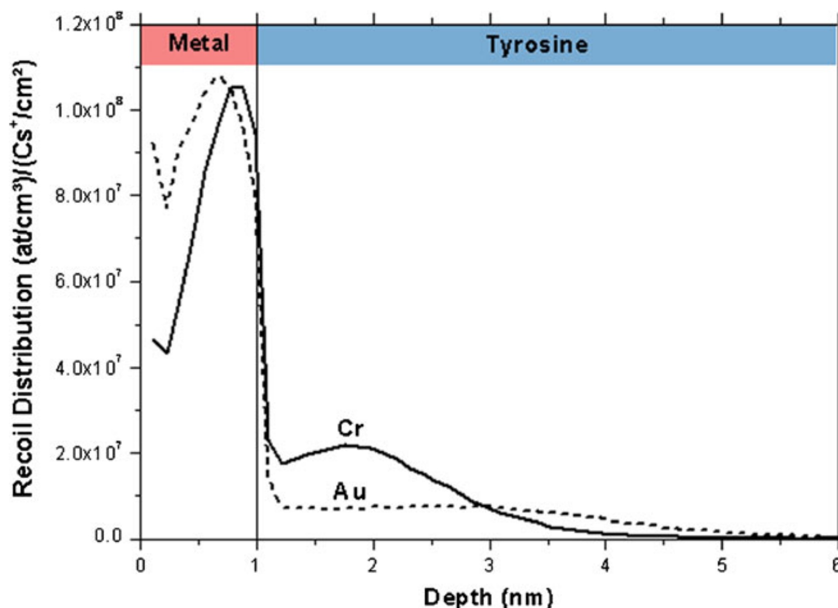

Figure 5. SRIM simulation of the recoil distribution of Cr and Au for a 1 nm metal overlayer on tyrosine

Table 1. Tyrosine, Gold, and Chromium Sputtering yields under a 500 eV Cs^+ Sputtering

Sample	Tyr S.Y (nm^3/ion)	Au S.Y. (nm^3/ion)	Cr S.Y (nm^3/ion)
Single layers	0.28	5.0×10^{-2}	1.6×10^{-2}
Bilayer Tyr/Au	0.31		
Bilayer Tyr/Cr	0.29		
Bilayer Au/Tyr	0.22		
Bilayer Cr/Tyr	0.089		
Trilayer Tyr/Au/Tyr 1st layer	0.25		
Trilayer Tyr/Au/Tyr 2nd layer	0.25		
Trilayer Tyr/Cr/Tyr 1st layer	0.27		
Trilayer Tyr/Cr/Tyr 2nd layer	0.082		

lower than on pure Tyr layers, it is about five times higher than on pure Cr layers. For Au capped layers, the Au injection is quite limited compared to the Cr case. Also, the sputtering yield difference between metal and Tyr is three times lower. Therefore, the second Tyr layer average sputtering yield is much less influenced by the Au concentration below the interface. Nevertheless, it remains surprising that virtually no change is measured in the Tyr sputtering yield. We speculate that a high Au concentration in the organic layer increases the Cs stopping power, bringing more energy near the surface, which maintains a high Tyr sputter rate, despite the high amount of recoil implanted overlayer atoms.

Depth Resolution

As the sputter velocity varies considerably at hybrid interfaces, due to the sputtering yield gap, giving an estimate of the depth resolution by solely inspecting the signal rise or decay is challenging. The Tyr molecular signals (e.g., at *m/z* 134 or 180) rise abruptly when the interface is reached, then increase much slower, leading to an overestimation of the interface width by using the 16%–84% criterion (this is the fluence needed to increase the signal from 16% to 84% of its steady state value). In spite of these limitations, we can estimate the depth resolution upper limit in an Au/Tyr hybrid interface by measuring the 16%–84% fluence on the $[Tyr\text{-}H]^-$ signal rise (1.87×10^{15} ions/cm²) and assuming a constant sputtering yield equal to the Tyr one (0.275 nm³/ion). Within these assumptions, the sputtered depth is about 5 nm, which is the actual depth resolution upper limit, considering that the real sputtering yield is certainly lower than that of pure Tyr. This result suggests that the depth resolution obtained with low energy Cs^+ is remarkably good, even on hybrid samples where the sputtering yield variations could induce severe interface roughening. No attempt was made to estimate the depth resolution on Cr/Tyr systems, since the sputtering yield difference between Cr and Tyr is even bigger than in an Au/Tyr interface.

Fragmentation

The Tyr layer was monitored by following the deprotonated ion $[Tyr\text{-}H]^-$, but three specific fragments were also monitored at *m/z* 134 ($C_8H_8NO^-$), *m/z* 119 ($C_8H_7O^-$), and *m/z* 93 ($C_6H_5O^-$). Since these fragments exhibit very similar ion intensities throughout depth profiling, only the largest one (*m/z* 134) is discussed. This fragment, obtained by a simple carboxylic acid group loss, remains a major fingerprint signal for Tyr. The intensity ratio between peaks at *m/z* 134 and 180 is defined as a "fragmentation index." The index increasing values indicate "harder" conditions, favoring functional groups loss in the Tyr molecule, while keeping most of its chemical structure intact. In pristine Tyr layers depth profiled with 500 eV Cs^+, this index stays constant at a 2.3 value. In the Cr/Tyr system (Figure 4.), the index rises up to 4 just beyond the hybrid interface, then returns to the pristine Tyr value (2.3). This implies that fragmentation conditions are harder just beyond the Cr layer, in regions where the Cr concentration is high. Again, the impacts between Cr atoms and Tyr molecules are likely to favor fragmentation. However, the molecules are not heavily damaged (i.e., graphitized) as confirmed by the specific high mass fragments signal intensity. Much less fragmentation is noticed on the Au/Tyr hybrid system: in the bilayers Au/Tyr shown in Figure 2a, the fragmentation index value just below the metal/Tyr interface rises up to 2.8, then decreases to 2.3. This is again consistent with a lower Au concentration below the hybrid interface, leading to fewer collisions between Au and Tyr molecules.

Conclusions

For the first time, it is shown that low energy Cs^+ bombardment is a reliable solution for hybrid depth profiling, without switching beams or changing parameters at the interface. The main reason for this successful hybrid depth profiling is the relatively low erosion rate difference between the organic and inorganic layers, as opposed to what is observed with cluster ion beams. The silicon substrate is reached within a reasonable time with only a weak loss of characteristic ion signals. Virtually no changes in sputtering yields are noticed before and after crossing the gold layer, whereas the sputtering yield is reduced by a factor of three after crossing the chromium layer. More fragmentation is also observed with chromium, but the remaining large fragments are still characteristic of the Tyr molecule, which retains most of its molecular integrity. The differences observed between the Au/Tyr and the Cr/Tyr hybrids are due to a stronger injection of energetic Cr atoms into the organic layer, compared to Au. Injected metal atoms contribute to more collisions with Tyr molecules, but they also significantly lower the Tyr layer erosion rate. A depth resolution estimate is difficult because of the important difference of sputtering yields between tyrosine and metals, but the Tyr signal rise at the Au/Tyr interface suggests a depth resolution better than 5 nm. The model samples presented here are quite simple, but these first

results are promising and could establish ToF-SIMS as a leading technique for the analysis of real-life hybrid devices.

Acknowledgments

The authors thank Mr. Corry Charlier from the University of Namur Electron Microscopy Service for his help in the PVD deposition of metallic layers. This service is member of the "Plateforme Technologique Morphologie-Imagerie". The authors also acknowledge the University of Namur PMR/LPME laboratory for providing access to the UHV evaporator used for depositing thin tyrosine layers.

References

1. Zheng, L., Wucher, A., Winograd, N.: Depth resolution during C60+ profiling of multilayer molecular films. Anal. Chem. **80**, 7363–7371 (2008)
2. Ninomiya, S., Ichiki, K., Yamada, H., Nakata, Y., Seki, T., Aoki, T., Matsuo, J.: Molecular depth profiling of multilayer structures of organic semiconductor materials by secondary ion mass spectrometry with large argon cluster ion beams. Rapid Commun. Mass Spectrom **23**, 3264–3268 (2009)
3. Shen, K., Wucher, A., Winograd, N.: Molecular depth profiling with argon gas cluster ion beams. J. Phys. Chem. C **119**, 15316–15324 (2015)
4. Gillen, G., Roberson, S.: Preliminary evaluation of an SF5+ polyatomic primary ion beam for analysis of organic thin films by secondary ion mass spectrometry. Rapid Commun. Mass Spectrom **12**, 1303–1312 (1998)
5. Weibel, D., Wong, S., Lockyer, N., Blenkinsopp, P., Hill, R., Vickerman, J.-C.: A C60 primary ion beam system for time of flight secondary ion mass spectrometry: its development and secondary ion yield characteristics. Anal. Chem. **75**, 1754–1764 (2003)
6. Shard, A.G., Green, F.M., Brewer, P.J., Seah, M.P., Gilmore, I.S.: Quantitative molecular depth profiling of organic delta-layers by C60 Ion sputtering and SIMS. J. Phys. Chem. B **112**, 2596–2605 (2008)
7. Wagner, M.S.: Molecular depth profiling of multilayer polymer films using time-of-flight secondary ion mass spectrometry. Anal. Chem. **77**, 911–922 (2005)
8. Winograd, N.: The magic of cluster SIMS. Anal. Chem. **77**, 142A–149A (2005)
9. Hada, M., Ibuki, S., Ninomiya, S., Seki, T., Aoki, T., Matsuo, J.: Evaluation of damage layer in an organic film with irradiation of energetic ion beams. Jpn. J. Appl. Phys. **49**, 036503 (2010)
10. Santoni, M.-P., Hanan, G.S., Hasenknopf, B.: Covalent multi-component systems of polyoxometalates and metal complexes: Toward multi-functional organic–inorganic hybrids in molecular and material sciences. Coord. Chem. Rev. **281**, 64–85 (2014)
11. Jorgensen, M., Norrman, K., Krebs, F.: Stability/degradation of polymer solar cells. Sol. Energ. Mat. Sol. Cells **92**, 686–714 (2008)
12. Heil, H., Steiger, J., Karg, S., Gastel, M., Ortner, H., von Seggern, H., Stossel, M.: Mechanisms of injection enhancement in organic light-emitting diodes through an Al/LiF electrode. J. Appl. Phys. **89**, 420 (2001)
13. Cumpson, P.J., Portoles, J.F., Barlow, A.J., Sano, N., Birch, M.: Depth profiling organic/inorganic interfaces by argon gas cluster ion beams: sputter yield data for biomaterials, in-vitro diagnostic and implant applications. Surf Interface Anal **45**, 1859–1868 (2013)
14. Shen, K., Mao, D., Garrison, B.J., Wucher, A., Winograd, N.: Depth profiling of metal overlayers on organic substrates with cluster SIMS. Anal. Chem. **85**, 10565–10572 (2013)
15. Seah, M.P.: Universal equation for argon gas cluster sputtering yields. J. Phys. Chem. C **117**, 12622–12632 (2013)
16. Niehuis, E.: In: Vickerman, J.C., Briggs, D. (eds.) ToF-SIMS: surface analysis by mass spectrometry, 2nd edn. IM Publications, Chichester (2012)
17. Yu, B.-Y., Chen, Y.-Y., Wang, W.-B., Hsu, M.-F., Tsai, S.-P., Lin, W.-C., Lin, Y.-C., Jou, J.-H., Chu, C.-W., Shyue, J.-J.: Depth profiling of organic films with x-ray photoelectron spectroscopy using C60+ and Ar+ Co-Sputtering. Anal. Chem. **80**, 3412–3415 (2008)
18. Houssiau, L., Mine, N.: Molecular depth profiling with reactive ions, or why chemistry matters in sputtering. Surf. Interface Anal. **43**, 146–150 (2010)
19. Brison, J., Vitchev, R.G., Houssiau, L.: Cesium/xenon co-sputtering at different energies during ToF-SIMS depth profiling. Nucl. Instr. Meth. Phys. Res. B **24**, 5159–5165 (2008)
20. Perego, M., Ferrari, S., Spiga, S., Fanciulli, M.: Nanocrystals depth profiling by means of Cs+ in negative polarity with dual beam ToF-SIMS. Appl. Surf. Sci. **203/204**, 110–113 (2003)
21. Kachan, M., Hunter, J., Kouzminov, D., Pivovarov, A., Gu, J., Stevie, F., Griffis, D.: O2+ versus Cs+ for high depth resolution depth profiling of III–V nitride-based semiconductor devices. Appl. Surf. Sci. **231/232**, 684–687 (2004)
22. Wittmaack, K.: Unravelling the secrets of Cs controlled secondary ion formation: evidence of the dominance of site specific surface chemistry, alloying and ionic bonding. Surf. Sci. Rep. **68**, 108–230 (2013)
23. Houssiau, L., Douhard, B., Mine, N.: Molecular depth profiling of polymers with very low energy ions. Appl. Surf. Sci. **255**, 970–972 (2008)
24. Mine, N., Douhard, B., Brison, J., Houssiau, L.: Molecular depth-profiling of polycarbonate with low-energy Cs+ ions. Rapid Commun. Mass Spectrom **21**, 2680–2684 (2007)
25. Terlier, T., Tiron, R., Gharbi, A., Chevalier, X., Veillerot, M., Martinez, E., Barnes, J.-P.: Investigation of block depth distribution in PS-b-PMMA block copolymer using ultra-low-energy cesium sputtering in ToFSIMS. Surf. Interface Anal. **46**, 83–91 (2014)
26. Iltgen, K., Bendel, C., Benninghoven, A., Niehuis, E.: Optimized time-of-flight secondary ion mass spectroscopy depth profiling with a dual beam technique. J. Vac. Sci. Technol. A. **15**, 460 (1997)
27. Brison, J., Mine, N., Wehbe, N., Gillon, X., Tabarrant, T., Sporken, R., Houssiau, L.: Molecular depth profiling of model biological films using low energy monoatomic ions. Int. J. Mass Spectrom. **311/322**, 1–7 (2012)
28. Kennedy, P., Postawa, Z., Garrison, B.J.: Dynamics displayed by energetic C60 bombardment of metal overlayers on an organic substrate. Anal. Chem. **85**, 2348–2355 (2013)
29. Available at: http://www.srim.org/. Accessed Aug 2015